Supporting Information

Fiber-shape $Na_3V_2(PO_4)_2F_3$@N-doped carbon as a cathode material with enhanced cycling stability for Na-ion batteries

Yunsha Li,[a, b] Xinghui Liang,[b] Guobin Zhong,[a] Chao Wang,[a] Shijia Wu,[a] Kaiqi Xu,*[,a] Chenghao Yang*,[b]

[a] *Electric Power Research Institute of Guangdong Power Grid Co., Ltd., Guangzhou, Guangdong 510080, China. E-mail: xukaiqi@yeah.net*

[b] *Guangzhou Key Laboratory for Surface Chemistry of Energy Materials, New Energy Research Institute, School of Environment and Energy, South China University of Technology, Guangzhou 510006, P. R. China. E-mail: esyangc@scut.edu.cn*

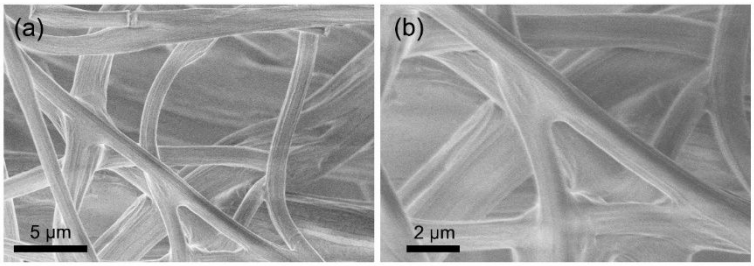

Figure S1. (a)-(b) SEM images of as-collected precursor fibers obtained by electrospinning with NVPF@C-2.

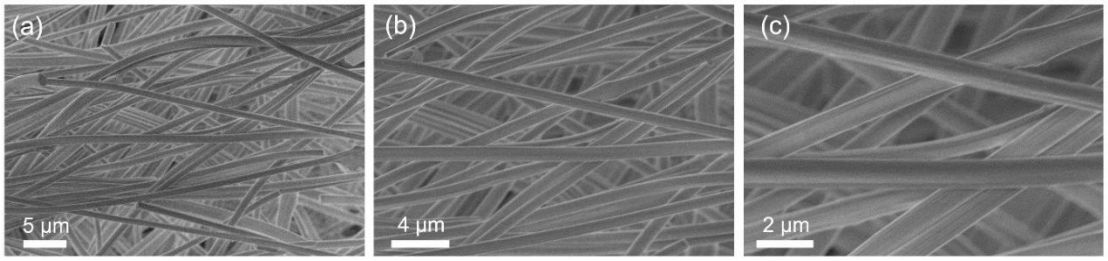

Figure S2. (a)-(c) SEM images of as-collected precursor fibers obtained by electrospinning with NVPF@C-3.

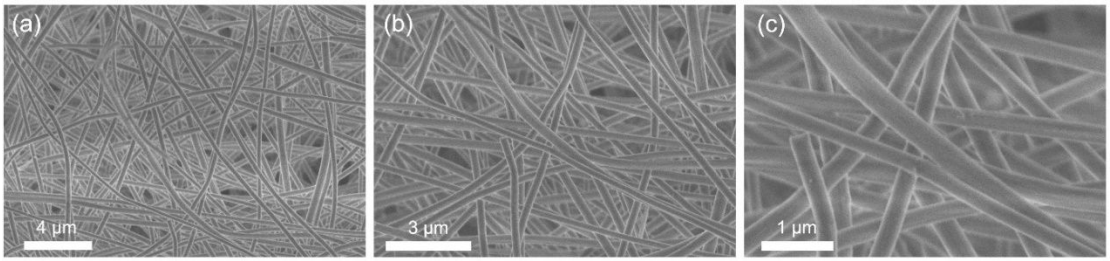

Figure S3. (a)-(c) SEM images of as-collected precursor fibers obtained by electrospinning with NVPF@C-4.

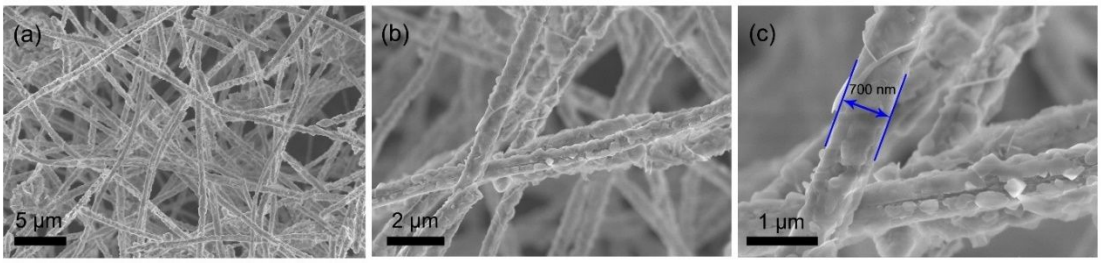

Figure S4. (a)-(c) SEM images of NVPF@C-2 after carbonized.

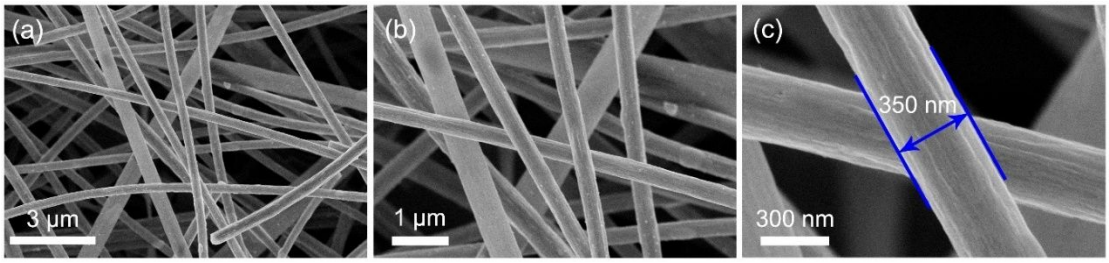

Figure S5. (a)-(c) SEM images of NVPF@C-4 after carbonized.

When the carbon content in the fiber is low (NVPF@C-2, Figure S4), the fiber diameter shrinks to 700 nm after heat treatment, but the carbon coating is insufficient to coat the active material so that particle precipitation occurs, which is not conducive to electron transport. When the carbon content in the fiber is high (NVPF@C-4, Figure S5), the fiber diameter is about 350 nm and no solid particles are precipitated. However, the carbon material itself lacks sodium storage activity in this voltage range, so excessive carbon coating will reduce the specific capacity of the material and affect the electrochemical performance of the composite.

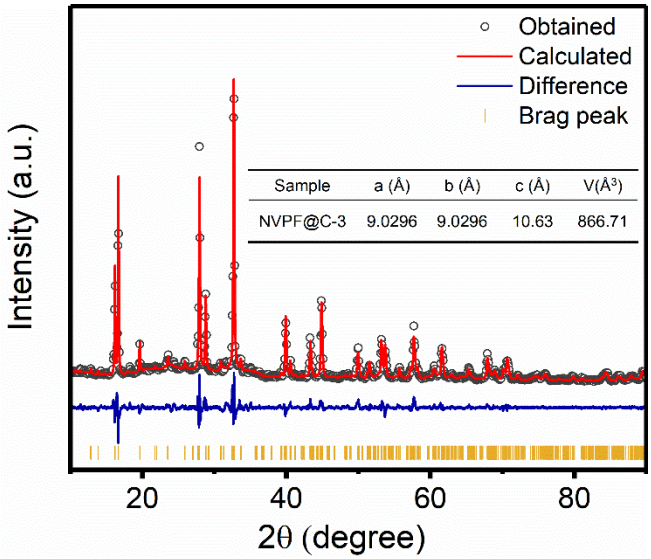

Figure S6. Rietveld refinement of the XRD patterns of NVPF@C-3.

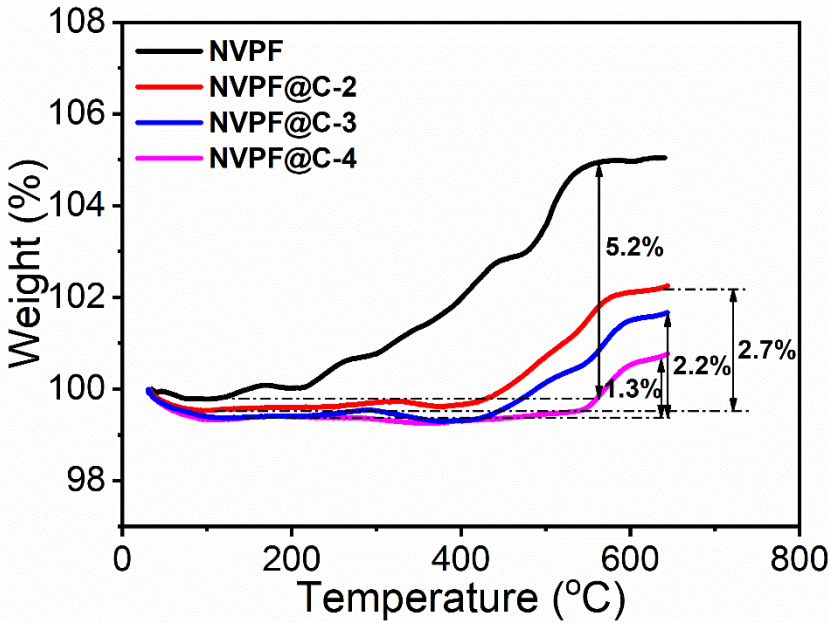

Figure S7. Thermogravimetric measurement profile of the pristine NVPF and NVPF@C.

Figure S7 displays the TGA results of three NVPF@C and pristine NVPF samples. The calculation method of carbon content in NVPF@C is introduced as follow. Based on the TG curve of pristine NVPF, 5.2% weight gain is observed when the sample is composed of 100% NVPF. The output ratio should be 1.052 (1.052=105.2%÷100%). Therefore, taking the TGA result of NVPF@C-2 as an example, 2.7% weight gain occurred, which means that the weight of the product after combustion is 102.7% times heavier than the original sample. The NVPF content in this sample is calculated to be 97.6% (97.6%=102.7%÷1.052), and the carbon content is 2.4% (2.4%=100%- 97.6%).

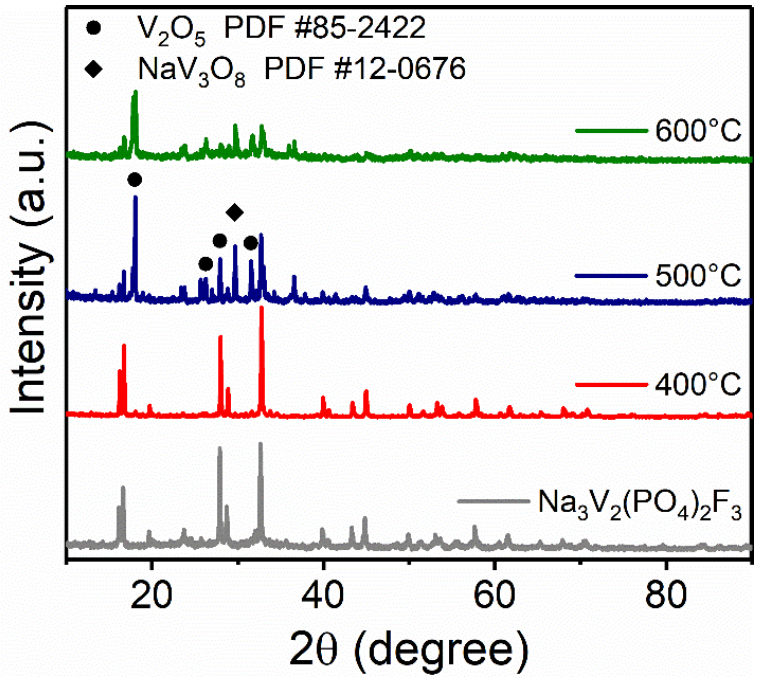

Figure S8. XRD patterns of NVPF@C after combustion at different temperature in air flow.

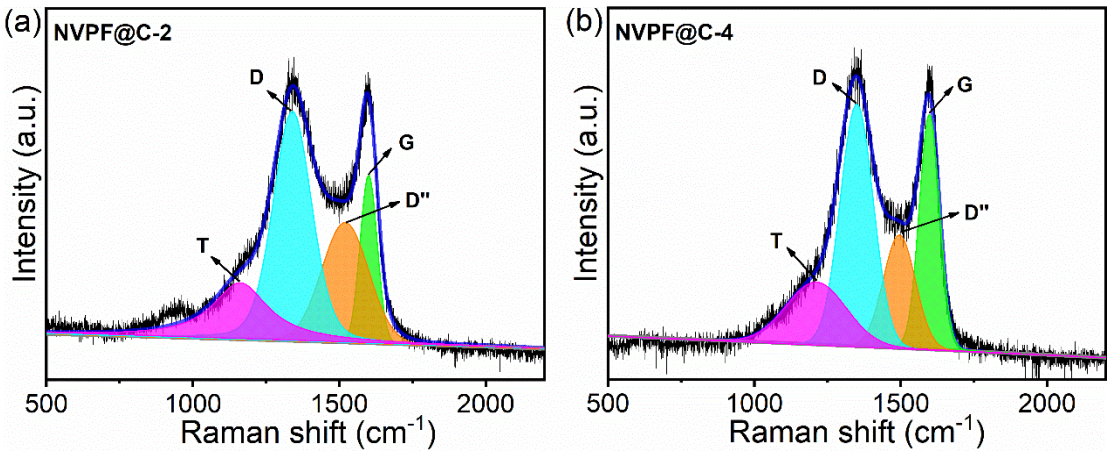

Figure S9. Raman spectra of (a) NVPF@C-2 and (b) NVPF@C-4.

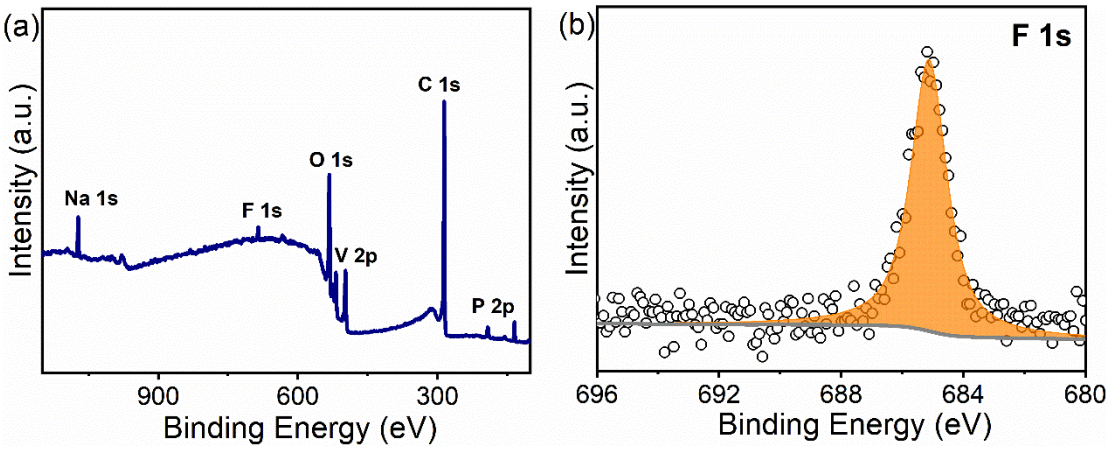

Figure S10. (a) Survey XPS and (b) high-resolution F 1s spectra of NVPF@C-3.

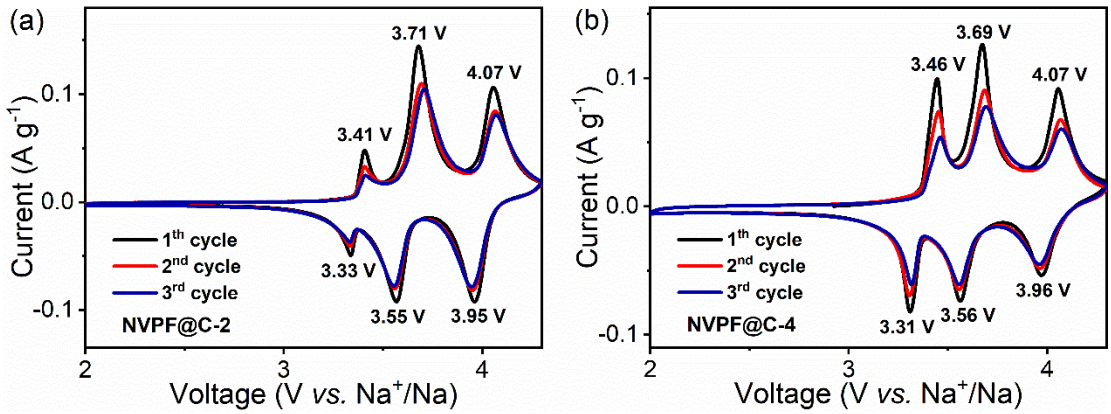

Figure S11. Cyclic voltammetry curves at a scan rate of 0.1 mV s^{-1} of (a) NVPF@C-2 and (b) NVPF@C-4.

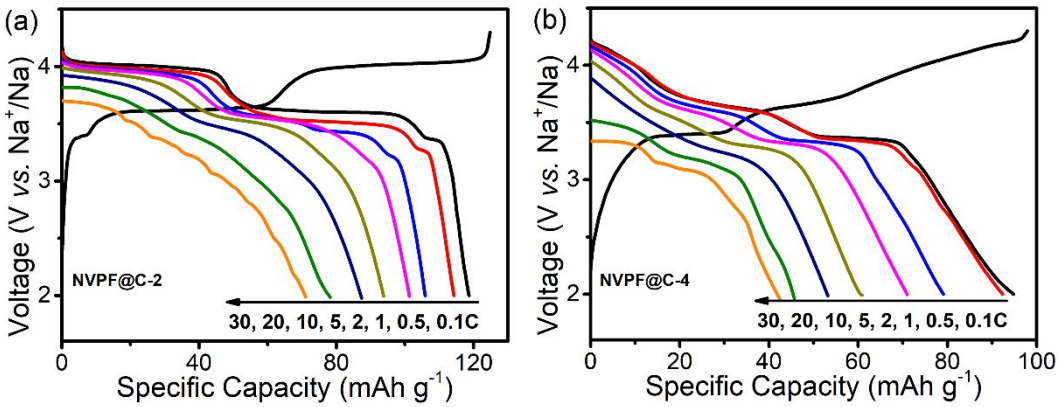

Figure S12. Charge-discharge profiles at different current density of (a) NCPF@C-2 and (b) NVPF@C-4.

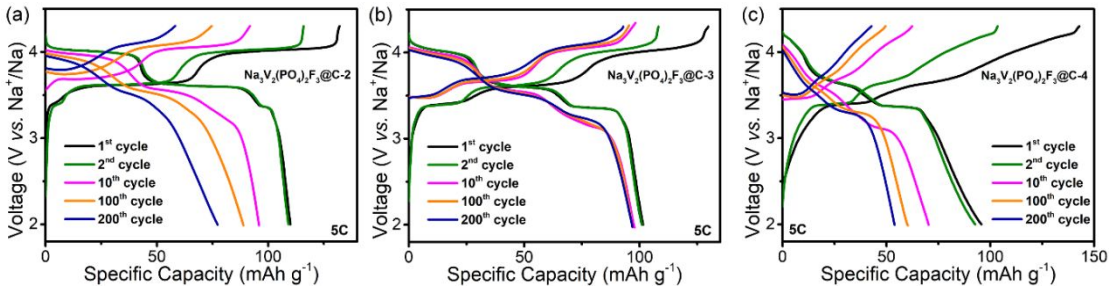

Figure S13. Charge-discharge curves of the (a) NVPF@C-2, (b) NVPF@C-3 and (c) NVPF@C-4 at 5 C in different cycles.

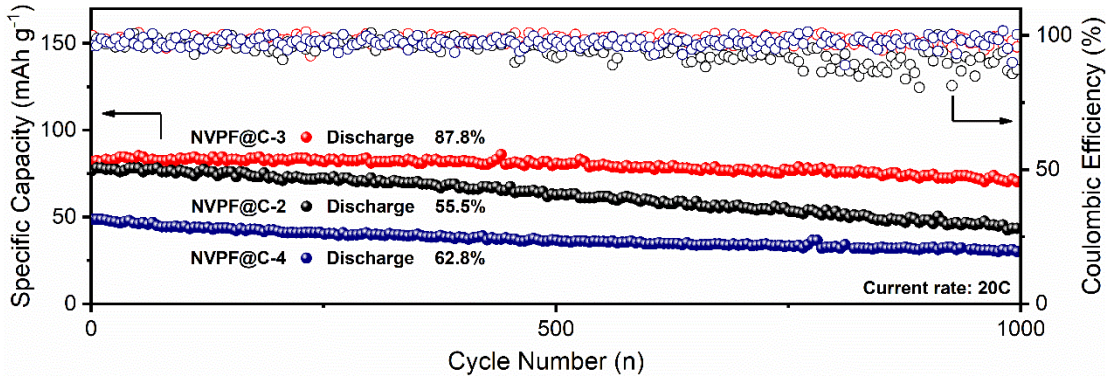

Figure S14. Cycling performance at 20 C of the NVPF@C cathode.

Table S1. Comparison of the results in this study with previously reported performance of other polyanion cathode material for sodium ion batteries.

Sample	Rate capacity (mA h g^{-1})	Cycle stability (mA h g^{-1})	Discharge potential (V *vs.* Na^+/Na)	Reference
$Na_3V_2(PO_4)_2F_3$	109.5 (0.1 C) 78.9 (30 C)	60.1 (50 C) (1500 cycles, 83.4%)	3.4, 3.6, 4.0	This work
$Na_3V_2(PO_4)_2F_3$	117 (0.1 C) 32 (10 C)	99.2 (0.2 C) (500 cycles, 94.5%)	3.95, 3.6	S1
$Na_3V_2(PO_4)_3$	113 (0.5 C) 81 (30 C)	78 (5 C) (2000 cycles, 68.4%)	3.4	S2
$NaVPO_4F$	120 (1 C) 82 (30 C)	107.1 (2 C) (1000 cycles, 96.5%)	3.42	S3
$NaVOPO_4$	144 (0.05 C) 58 (5 C)	75 (0.5 C) (1000 cycles, 67%)	3.5	S4
$Na_7V_4(P_2O_7)_4PO_4$	92 (0.05 C) 70.2 (10 C)	81.4 (0.5 C) (300 cycles, 92.1%)	3.53	S5
$Na_3V(PO_3)_3N$	73 (0.1 C) 61.3 (10 C)	48.9 (0.5 C) (3000 cycles, 67%)	4	S6
Na_2FePO_4F	103.2 (0.1 C) 66.8 (4 C)	56.6 (4 C) (1000 cycles, 84.7%)	3.16, 2.95	S7
$Na_4Fe_3(PO_4)_2(P_2O_7)$	128 (0.1 C) 93 (20 C)	62.9 (10 C) (6000 cycles, 62.3%)	3.20, 2.88	S8
$NaFe(SO_4)_2$	80 (0.1 C) 40 (2 C)	78 (0.1 C) (80 cycles, 97.5%)	3	S9
$Na_2Fe_2(SO_4)_3$	102 (0.05 C) 59 (20 C)	99.5 (0.05 C) (5 cycles, 97.5%)	3.8	S10

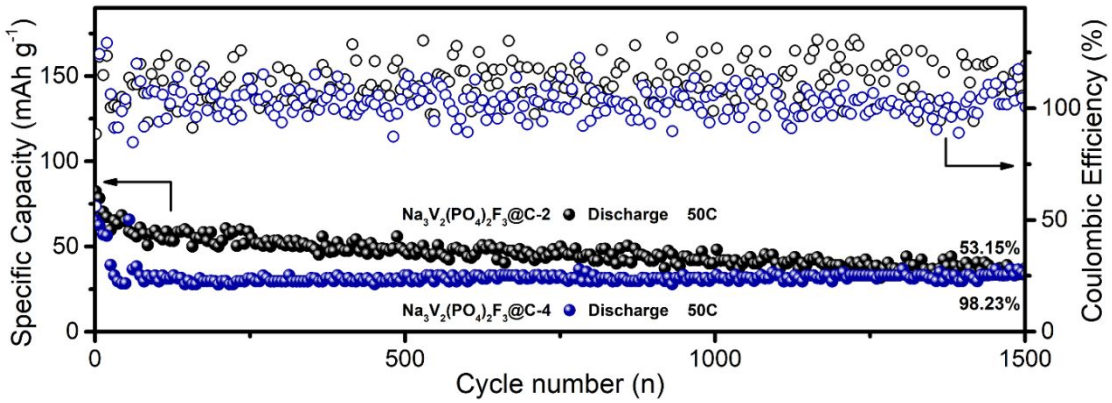

Figure S15. Cycling performance at 50 C of NVPF@C-2 and NVPF@C-4 cathode.

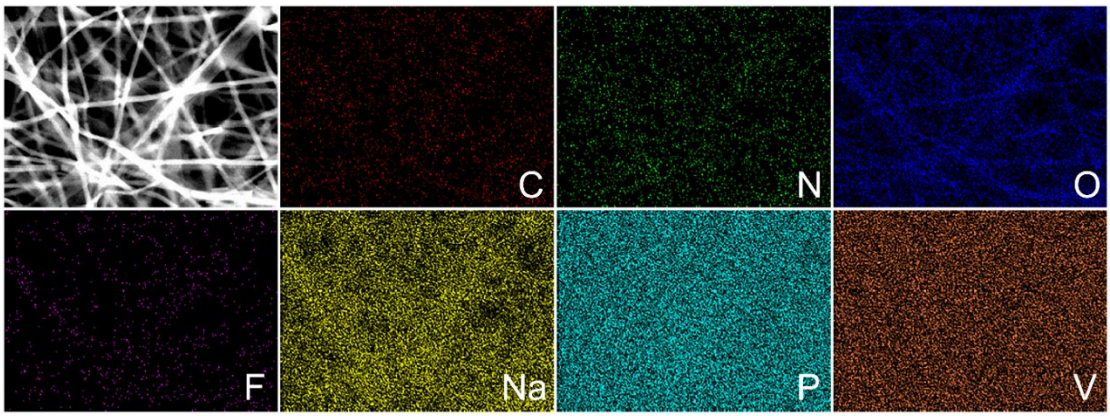

Figure S16. EDS mapping images of NVPF@C-3 fibers after 100 cycles.

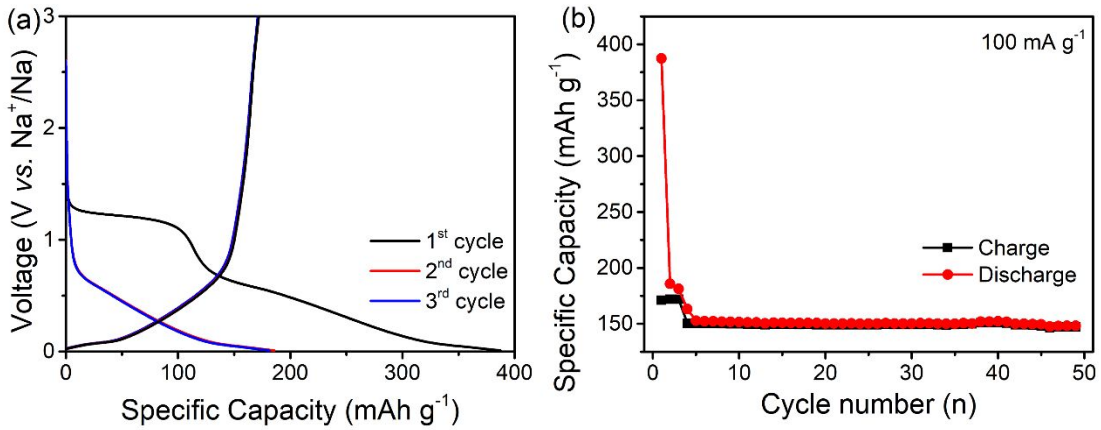

Figure S17. (a) Charge-discharge profiles and (b) cycling performance at 100 mA g^{-1} of hard carbon.

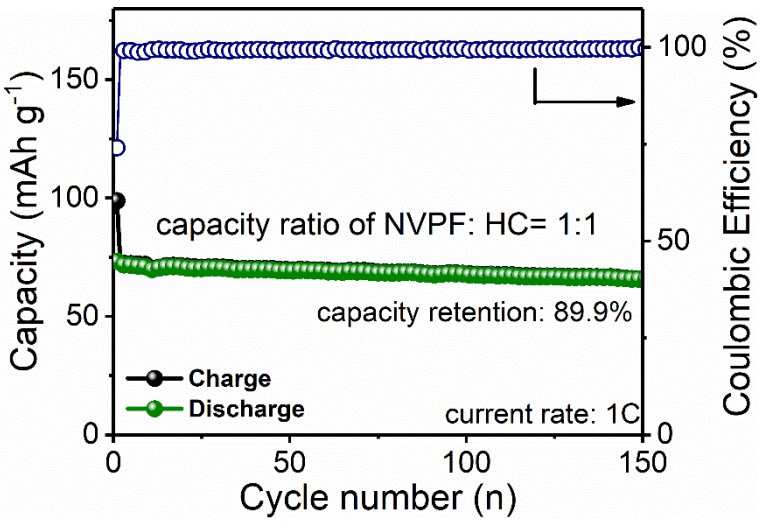

Figure S18. Cycling performance of the NVPF@C-3||HC full cell.

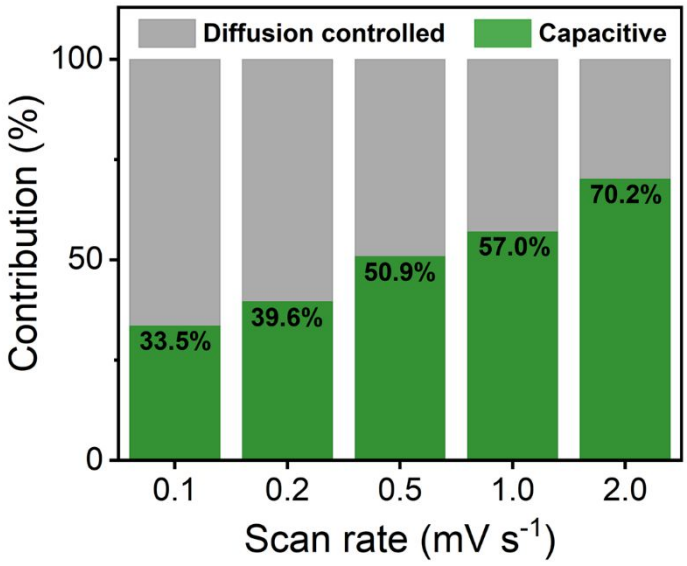

Figure S19. Diagram of capacitive contribution to the total capacity of NVPF@C-3.

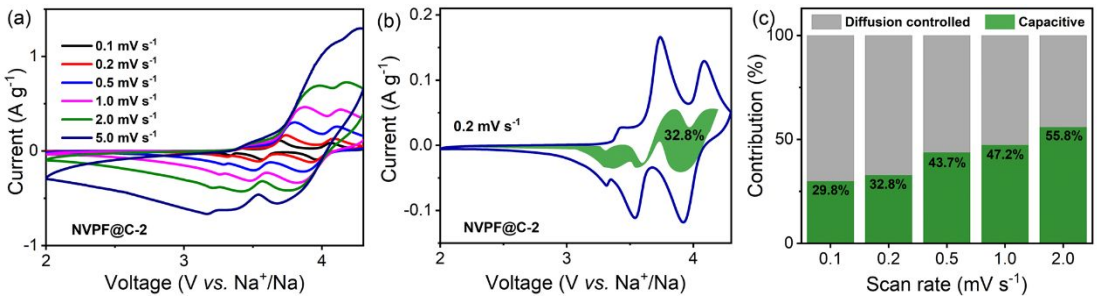

Figure S20. (a) CV curves at different sweep rates, from 0.1 to 5 mV s^{-1}, (b) capacitive contribution (shaded region) to total current at a scan rate of 0.2 mV s^{-1}, and (c) diagram of capacitive contribution to the total capacity of NVPF@C-2.

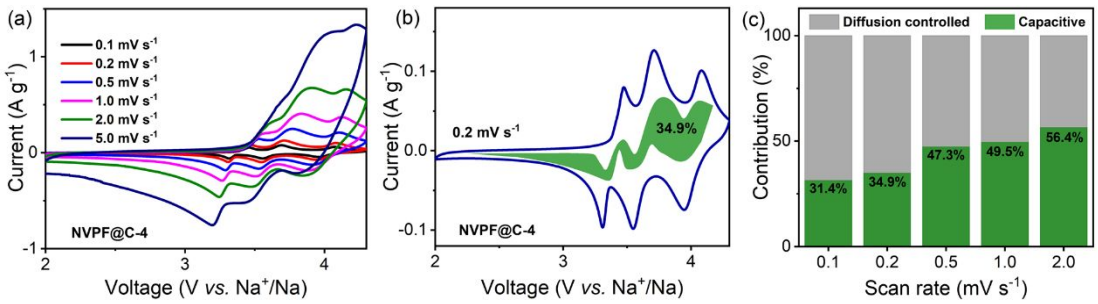

Figure S21. (a) CV curves at different sweep rates, from 0.1 to 5 mV s^{-1}, (b) capacitive contribution (shaded region) to total current at a scan rate of 0.2 mV s^{-1}, and (c) diagram of capacitive contribution to the total capacity of NVPF@C-4.

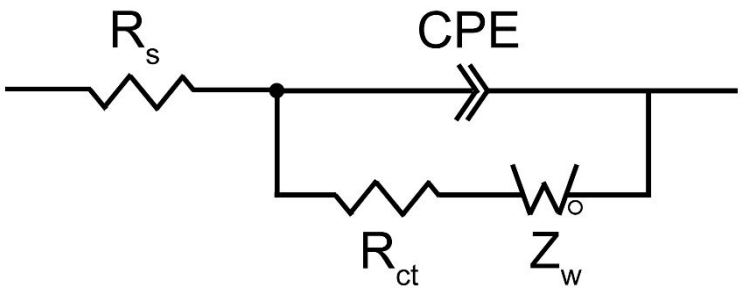

Figure S22. Equivalent circuit used for fitting the experimental EIS data.

Figure S22 shows the equivalent circuit model or simulations of all Nyquist plots, where R_s stands for the Ohmic resistance and R_{ct} is ascribed to the charge transfer resistance, while CPE refers to the constant phase angle element and Z_w represents the Warburg impedance, respectively.

Table S2. The impedance parameters from the simulated equivalent circuit and sodium diffusion coefficients of NVPF@C.

Sample	Cycle number	R_s (Ω)	R_{ct} (Ω)	σ_w (Ω $s^{-1/2}$)	D_{Na} (cm^2 s^{-1})
NVPF@C-2	Pristine	1.93	157.7	111.09	8.01×10^{-14}
	50	1.13	666.8		
	100	4.37	1323		
NVPF@C-3	Pristine	2.46	122.4	73.59	1.83×10^{-13}
	50	2.91	477.2		
	100	5.56	732.4		
NVPF@C-4	Pristine	3.89	225.1	204.74	2.36×10^{-14}
	50	3.31	688.7		
	100	5.63	868.4		
Bare NVPF	Pristine	3.40	246.9	212.97	2.18×10^{-14}
	50	3.16	1215.0		
	100	2.62	1826.0		

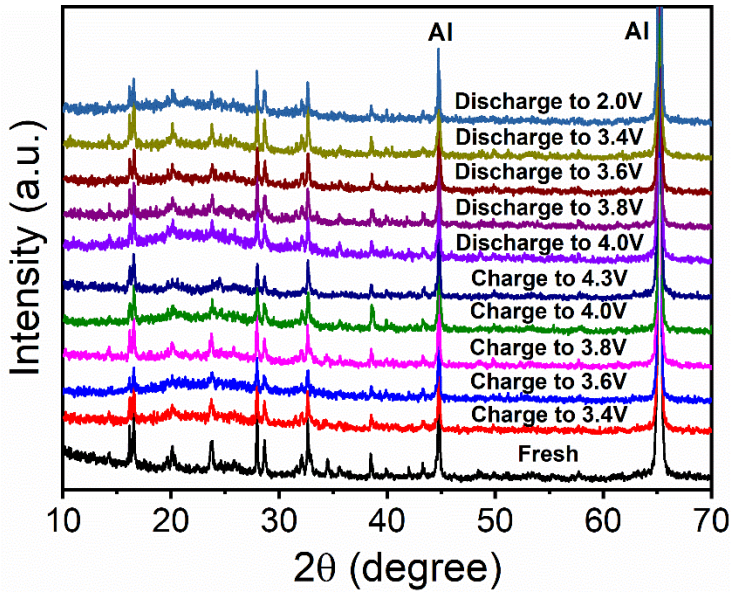

Figure S23. *Ex-situ* XRD patterns of the NVPF@C-3 electrode at selected charged/discharged stages in the initial cycles.

Figure S23 illustrated the *ex-situ* XRD curves of NVPF@C-3 during the initial cycle. The constant unchanged peaks located at 44.8° and 65.2° are ascribed to aluminum substrate. Compared the XRD patterns at different potential voltage, there is little significant variation observed about peak positions of $Na_3V_2(PO_4)_2F_3$, suggesting the excellent structure stability, which is beneficial to achieve an ultra-high rate property and ultra-long cycling stability.

Table S3. The content of C and N in NVP@C-3 measured by elemental analysis of CHN/O test.

Sample	N Area	C Area	H Area	N (%)	C (%)	H (%)
NVPF@C-3	1376	3155	836	0.76	3.02	0.298

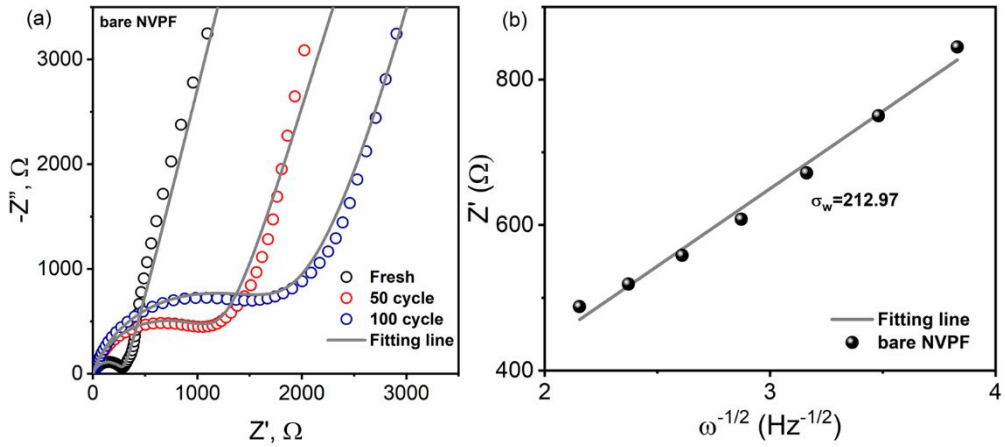

Figure S24. (a) Recorded impedance spectra and (b) the relationship between Z_{re} and $\omega^{-1/2}$ of bare NVPF.

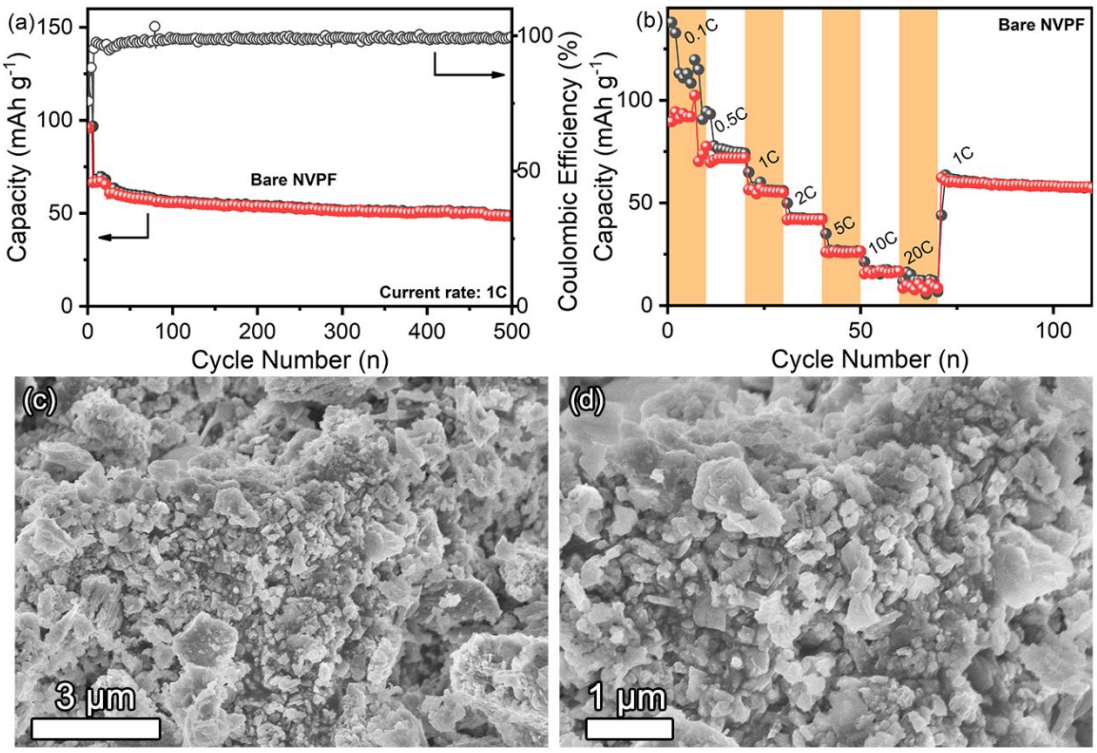

Figure S25. (a) Cyclic and (b) rate performance and (c-d) SEM images before cycling of bare NVPF.

Reference

(S1) Qi, Y.; Mu, L.; Zhao, J.; Hu, Y.-S.; Liu, H.; Dai, S., pH-Regulative Synthesis of $Na_3(VPO_4)_2F_3$ Nanoflowers and Their Improved Na Cycling Stability. *J. Mater. Chem. A.* **2016,** *4*, 7178-7184.

(S2) Jiang, Y.; Yang, Z.; Li, W.; Zeng, L.; Pan, F.; Wang, M.; Wei, X.; Hu, G.; Gu, L.; Yu, Y., Nanoconfined Carbon-Coated $Na_3V_2(PO_4)_3$ Particles in Mesoporous Carbon Enabling Ultralong Cycle Life for Sodium-Ion Batteries. *Adv. Energy Mater.* **2015,** *5*, 1402104.

(S3) Jin, T.; Liu, Y.; Li, Y.; Cao, K.; Wang, X.; Jiao, L., Electrospun $NaVPO_4F$/C Nanofibers as Self-Standing Cathode Material for Ultralong Cycle Life Na-Ion Batteries. *Adv. Energy Mater.* **2017,** *7*, 1700087.

(S4) Fang, Y.; Liu, Q.; Xiao, L.; Rong, Y.; Liu, Y.; Chen, Z.; Ai, X.; Cao, Y.; Yang, H.; Xie, J., A Fully Sodiated $NaVOPO_4$ with Layered Structure for High-Voltage and Long-Lifespan Sodium-Ion Batteries. *Chem.* **2018,** *4*, 1167-1180.

(S5) Fang, W.; An, Z.; Xu, J.; Zhao, H.; Zhang, J., Superior Performance of $Na_7V_4(P_2O_7)_4PO_4$ in Sodium Ion Batteries. *RSC Adv.* **2018,** *8*, 21224-21228.

(S6) Kim, J.; Yoon, G.; Lee, M. H.; Kim, H.; Lee, S.; Kang, K., New 4V-Class and Zero-Strain Cathode Material for NA-Ion Batteries. *Chem. Mater.* **2017,** *29*, 7826-7832.

(S7) Deng, X.; Shi, W.; Sunarso, J.; Liu, M.; Shao, Z., A Green Route to a Na_2FePO_4F-Based Cathode for Sodium Ion Batteries of High Rate and Long Cycling Life. *ACS Appl. Mater. Interfaces.* **2017,** *9*, 16280-16287.

(S8) Yuan, T.; Wang, Y.; Zhang, J.; Pu, X.; Ai, X.; Chen, Z.; Yang, H.; Cao, Y., 3D

Graphene Decorated $Na_4Fe_3(PO_4)_2(P_2O_7)$ Microspheres as Low-Cost and High-Performance Cathode Materials for Sodium-Ion Batteries. *Nano Energy.* **2019,** *56*, 160-168.

(S9) Singh, P.; Shiva, K.; Celio, H.; Goodenough, J. B., Eldfellite, $NaFe(SO_4)_2$: An Intercalation Cathode Host for Low-Cost Na-Ion Batteries. *Energy Environ. Sci.* **2015,** *8*, 3000-3005.

(S10) Barpanda, P.; Oyama, G.; Nishimura, S.; Chung, S. C.; Yamada, A., A 3.8-V Earth-Abundant Sodium Battery Electrode. *Nat Commun.* **2014,** *5*, 4358.